# Super-Resolution Fluorescence Imaging of *Arabidopsis thaliana* Transfer Cell Wall Ingrowths Using Pseudo-Schiff Labelling Adapted for the Use of Different Dyes

Angus E. Rae [a #], Xiaoyang Wei [a], Neftali Flores-Rodriguez [b], David W. McCurdy [a] and David A. Collings [a *]

[a] School of Environmental and Life Sciences, University of Newcastle, Callaghan, NSW 2308, Australia.

[b] Australian Centre for Microscopy and Microanalysis, University of Sydney, Sydney, NSW 2006, Australia.

**Running title:**

Super-Resolution Imaging of Cell Wall Ingrowths

**Corresponding author:**

D.A. Collings

School of Environmental and Life Sciences

The University of Newcastle

Callaghan, NSW 2308, Australia

E-mail: david.collings@newcastle.edu.au

**Subject Areas:**

11 - New methodology

1 - Growth and development

**Manuscript information:**

6 black and white figures

1 colour figure

1 table

0 supplementary figure

3 supplementary movies

**Super-Resolution Fluorescence Imaging of *Arabidopsis thaliana* Transfer Cell Wall Ingrowths Using Pseudo-Schiff Labelling Adapted for the Use of Different Dyes**

Angus E. Rae [a #], Xiaoyang Wei [a], Neftali Flores-Rodriguez [b], David W. McCurdy [a *] and David A. Collings [a *]

[a] School of Environmental and Life Sciences, University of Newcastle, Callaghan, NSW 2308, Australia.

[b] Australian Centre for Microscopy and Microanalysis, University of Sydney, Sydney, NSW 2006, Australia.

[*] **Corresponding authors**

David Collings, E-mail david.collings@newcastle.edu.au

David McCurdy, E-mail david.mccurdy@newcastle.edu.au

[#] Current address:

Research School of Biology

The Australian National University

Canberra ACT 2601 Australia

**Keywords**

*Arabidopsis thaliana*; Phloem parenchyma transfer cells; Plant cell walls; Pseudo-Schiff labelling; STED microscopy; Wall ingrowths

**Abstract**

To understand plant growth and development, it is often necessary to investigate organisation of plant cells and plant cell walls. Plant cell walls are often fluorescently labelled for confocal imaging with the dye propidium iodide using a pseudo-Schiff reaction. This reaction binds free amine groups on dye molecules to aldehyde groups on cellulose that result from oxidation with periodic acid. We tested a range of fluorescent dyes carrying free amine groups for their ability to act as pseudo-Schiff reagents. Using the low-pH solution historically used for the Schiff reaction, these alternative dyes failed to label cell walls of *Arabidopsis* cotyledon vascular tissue as strongly as propidium iodide but replacing the acidic solution with water greatly improved fluorescence labelling. Under these conditions, rhodamine-123 provided improved staining of plant cell walls compared to propidium iodide. We also developed protocols for pseudo-Schiff labelling with ATTO 647N-amine, a dye compatible for super-resolution Stimulated Emission Depletion (STED) imaging. ATTO 647N-amine was used for super-resolution imaging of cell wall ingrowths that occur in phloem parenchyma transfer cells of *Arabidopsis*, structures whose small size is only slightly larger than the resolution limit of conventional confocal microscopy. Application of surface rendering software demonstrated the increase in plasma membrane surface area as a consequence of wall ingrowth deposition and suggests that STED-based approaches will be useful for more detailed morphological analysis of wall ingrowth formation. These improvements in pseudo-Schiff labelling for conventional confocal microscopy and STED imaging will be broadly applicable for high resolution imaging of plant cells walls.

## Introduction

The existence of the cell wall is a fundamental characteristic of plant cells. In their simplest form, cell walls are a layer of cellulose microfibrils and other polysaccharides deposited outside the plant cell's plasma membrane. Within this simplistic description, however, great diversity exists in the chemical and structural features of plant cell walls, and this diversity contributes to the roles played by the wall in providing structural support, shape determination and protection. Examples of this diversity include water-conducting xylem elements in which lignified and thickened secondary cell walls arranged in rings or spirals allow for continued elongation of these cells even after they have undergone programmed cell death (Schuetz et al. 2013); stomatal guard cells, where the asymmetric deposition of cellulose microfibrils allows changes in turgor pressure to be converted into stomatal movements, thus allowing the control of gas exchange (Rui and Anderson 2016); and transfer cells, where intricate wall ingrowth networks enhance plasma membrane surface area, increasing nutrient transport (McCurdy et al. 2008). In such examples, the organisation and composition of cell wall determine the overall properties of the specialised cell types (Doblin et al. 2010). Thus, understanding cell wall structure represents a vital element towards understanding plant cell function.

Recent advances in fluorescence imaging of plant cell walls has been achieved through the use of optimised fluorescent proteins (Stoddard and Rolland 2019), fluorescent dyes specific for cellulose (Anderson et al. 2010) and lignin (Kapp et al. 2015), and with click chemistry (Lion et al. 2017). The Schiff reaction has also been used for labelling of cell walls (Haseloff 2003), allowing the covalent binding of free amine groups to free aldehydes to form a Schiff base, or imine. In the traditional form of this reaction, the addition of sulfurous acid ($SO_2$) decolourises the magenta-coloured basic fuchsin (also known as pararosaniline) but on addition of aldehydes, the dye binds to the aldehyde groups and the magenta colour is recovered (Schiff 1866). The solution of pararosaniline and $SO_2$, termed Schiff's reagent, allows detection and quantification of free aldehydes in solutions and tissues. Schiff's reagent has since been modified by the use of different dyes that contain free amine groups, with such alternative dyes known as pseudo-Schiff reagents (Dapson 2016).

One of the principal applications of pseudo-Schiff reagents is to specifically stain cellular components such as carbohydrates or DNA through the formation of free aldehydes on structures of interest (Chieco and Derenzini 1999). Schiff labelling of carbohydrates, known as the periodic acid-Schiff (PAS) technique, was first described in 1948 (McManus 1948). In plant tissue, 1% periodic acid can be used to oxidise free, vicinal (adjacent) -OH groups along the surface of cellulose and other carbohydrates to free aldehydes that can then be bound covalently to a pseudo-Schiff reagent (Baum 2008). Although the periodic acid-Schiff approach

typically uses coloured dyes for transmitted light imaging, Haseloff achieved high resolution confocal imaging through the introduction of the free amine-containing fluorescent dye propidium iodide and high-refractive index, chloral hydrate-based mounting solutions suitable for three-dimensional (3D) imaging (Haseloff 2003). The intense and photostable propidium iodide labelling in the PAS technique greatly improved the depths to which optical sectioning was possible, allowing high-resolution 3D reconstruction of whole plant organs. The method has proved to be highly effective and has been used extensively and modified (Moreno et al. 2006, Truernit et al. 2008, Truernit and Palauqui 2009, Wuyts et al. 2010, Nguyen and McCurdy 2015, Coiro and Truernit 2017, Mendocilla Sato and Baroux 2017, Nguyen et al. 2017, Wei et al. 2020). Despite widespread use for the fluorescent labelling of cell walls, the original method and its variants all use reactions and solutions based on Schiff's original study, and have been limited to the use of propidium iodide as the fluorescent pseudo-Schiff reagent. Several questions, however, might be raised concerning its use. First, propidium iodide is a DNA-binding molecule whose structure is closely related to the well-recognised mutagen ethidium bromide and has itself been used as a mutagenic agent in yeast (Fukunaga and Yielding 1980). And second, propidium iodide binds to several locations within the cell, not only binding to DNA (Suzuki et al. 1997) but also to the plant cell wall (Haseloff et al. 1999, Rounds et al. 2011) which might confound labelling reactions.

Other fluorescent dyes have been used in Schiff-based labelling of carbohydrates. Basic fuchsin has traditionally been used for pseudo-Schiff labelling of the cell wall for conventional light microscopy (Jensen 1962) including confocal imaging of cell walls (Davis et al. 1986). A potential problem with this approach, however, is that basic fuchsin is, in its own right, a fluorescent stain for lignified cell walls (Kapp et al. 2015), an effect which might confound its use. The underlying chemistry of the Schiff reaction suggests that any fluorescent dye whose chemical structure includes a free amine group should behave as a Schiff reagent (Dapson 2016) and might be used in the labelling of plant cell walls. Indeed, this was alluded to by Haseloff where it was suggested that the method would work "with fluorescent pseudo-Schiff reagents, such as propidium iodide" (Haseloff 2003). Therefore, it is plausible that there are numerous alternatives to propidium iodide that are safer and/or more effective for labelling of plant cell walls, which have yet to be tested.

In this study, we imaged wall ingrowth deposition in phloem parenchyma transfer cells of cotyledons and leaves in *Arabidopsis thaliana* (Arabidopsis). Electron microscopy has demonstrated the complex shape and small size of these specialised cell wall structures (Haritatos et al. 2000, Amiard et al. 2005, Maeda et al. 2006, Edwards et al. 2010, Adams et al. 2014, Maeda et al. 2014). While these ingrowths have been visualised and quantified by

confocal microscopy with a pseudo-Schiff labelling protocol using propidium iodide (Nguyen and McCurdy 2015, Nguyen et al. 2017, Wei et al. 2020), the widths and depths of the ingrowths approach the lateral and axial resolutions of conventional fluorescence microscopy. This limitation means that assessing changes in wall ingrowth structure during experimental treatments can be difficult. We investigated alternative fluorescent pseudo-Schiff reagents for labelling plant cell walls using the Arabidopsis phloem parenchyma transfer cells system. We identified the deleterious effects of the low pH pseudo-Schiff solution historically used for imaging with propidium iodide. Replacing this acidic buffer with water increased the efficiency of propidium iodide labelling and enabled a greater range of alternative fluorescent dyes to be used. Rhodamine-123, in particular, provided improved 3D imaging of the wall ingrowths. Furthermore, the improvement of the Schiff labelling technique also enabled optimisation of procedures for super-resolution imaging of the cell wall with stimulated emission depletion (STED) microscopy using the dye ATTO 647N-amine. Using this approach coupled with deconvolution, we achieved images of wall ingrowths that approached the clarity of those obtained with scanning electron microscopy. Application of surface rendering software enabled estimation of the surface area of the ingrowth network, thus providing quantitative assessment of the extent of wall ingrowth deposition. The developments reported here for improved pseudo-Schiff labelling and super-resolution microscopy will be widely applicable for imaging cell wall structures in other cell types.

## Results

*Alternative fluorescent dyes for propidium iodide*

Nine fluorescent Schiff reagents including propidium iodide that contain free amine groups (Fig. 1) were used to label both vascular bundles and phloem parenchyma transfer cells in Arabidopsis cotyledons. Six of these alternative dyes (acriflavine, auramine O, basic fuchsin, neutral red, rhodamine-123 and safranin O) were previously identified as pseudo-Schiff dyes (Kasten 1958, Kasten 1959), while two are amine derivatives of ATTO 565 and ATTO 647N, dyes that have only recently been developed for super-resolution microscopy (Willig et al. 2007, Sednev et al. 2015). Initial tests focused on comparing the first six of these dyes with propidium iodide, with the aim of developing methods for subsequent use with ATTO 565-amine and ATTO 647N-amine.

Dye solutions (1 mg/mL in water) were diluted to 100 µg/mL in pseudo-Schiff solution (100 mM $Na_2S_2O_5$ in 0.15 M HCl) and used to label cell walls of 12-18 day-old fixed and bleach-cleared Arabidopsis cotyledons, following the modified pseudo-Schiff propidium iodide labelling

procedure (Nguyen and McCurdy 2015). Each labelled sample was imaged by confocal microscopy. Averaging the gain settings required for maximum non-saturating imaging of vascular tissue in the cotyledons allowed for comparisons of fluorescence labelling intensity between samples. As more intensely fluorescent images required lower gain settings, we defined 'brightness' as the value of 1000 minus the gain value so that more intense images had a higher brightness score. When brightness values were averaged for vascular tissue labelling with the seven different dyes (Fig. 2A), propidium iodide and rhodamine-123 gave the brightest staining with brightness scores averaging over 500, whereas the remaining five dyes showed much lower labelling intensity. The values of between 250 and 450 for basic fuchsin, safranin O, neutral red and auramine O corresponded to very weak fluorescent labelling.

*Effects of pH on the Schiff reaction*

The variability of staining (Fig. 2) raised the question as to why these dyes performed relatively poorly compared to propidium iodide when they contained at least one free amine group and should act as Schiff-reagents to strongly label oxidised cell walls. In the original Schiff reaction, $SO_2$ produced by the reaction of sodium or potassium metabisulfite with HCl decolourised basic fuchsin (pararosaniline) (Schiff 1866), with this colour change used to measure aldehydes (Feulgen and Rossenbeck 1924). However, neither propidium iodide nor any of the other Schiff reagents were decolourised by the $SO_2$. This observation suggested that the pseudo-Schiff solution might not be required in the propidium iodide labelling reaction. Further, the low pH pseudo-Schiff solution (pH ~ 1.5) might have a negative effect on the labelling reaction because it would protonate primary amine groups on the dye molecules, preventing the Schiff reaction from proceeding. This possibility was suggested by the observation that the alternative Schiff reagents with higher pKa values than propidium iodide labelled less well (Fig. 2A, Table 1). To test this possibility, dye solutions (1 mg/mL in water) were diluted to 100 µg/mL in water rather than pseudo-Schiff solution. Cotyledons stained in this way showed signs of significant over-staining, with strong background fluorescence. Because of this, each dye was re-tested at different concentrations and staining times to determine optimum conditions when diluted in water. This analysis showed that for each dye, with the exception of auramine O, a substantially lower dye concentration, sometimes as low as 1.0 µg/mL, was required for optimum staining when diluted in water, compared to the 100 µg/mL required when diluted in the pseudo-Schiff solution (Table 1).

To further compare the effect of replacing the pseudo-Schiff solution with water as the dye solvent, the labelling brightness of samples stained at the optimum conditions when diluted in water were compared to samples labelled in pseudo-Schiff solution under the same conditions. Even at these lower dye concentrations, the effect of raising pH was substantial, with all dyes

except acriflavine showing either modest (for example, propidium iodide) or substantial (basic fuchsin, safranin O, auramine O) increases in labelling brightness (Fig. 2B, black bars). The increase in labelling was more pronounced for dyes with less acidic pKa values, as would be expected were the acidic pseudo-Schiff solution limiting reaction effectiveness. Acriflavine was the only exception: samples labelled with this dye showed no intensity differences between water and pseudo-Schiff solution, a result that fits with the low pKa of acriflavine which would mean that the dye remained unprotonated in the acidic pseudo-Schiff solution. Despite differences in the strength of labelling, no differences were observed in the labelling patterns of the dyes.

Differences in labelling efficiency were readily visible in images of vascular tissue of 12-day–old cotyledons stained with either propidium iodide or rhodamine-123 (Fig. 3). While water-based labelling showed some increase for propidium iodide labelling (Fig. 3A, B), labelling with rhodamine-123 was much stronger in water (Fig. 3C) than in the acid pseudo-Schiff solution (Fig. 3D). One further difference noted was that the samples labelled in water were considerably less fragile, probably due to reduced exposure to acidic conditions.

*The importance of the mounting solution*

The original protocol for pseudo-Schiff labelling with propidium iodide (Haseloff 2003), and subsequent modifications to this (Truernit et al. 2008, Wuyts et al. 2010, Nguyen and McCurdy 2015), mounted labelled samples in either chloral hydrate or chloral hydrate hardened with gum arabic. The high refractive index of this mounting solution aids in 3D imaging of the plant tissue, as well as providing additional clearing of the sample. When propidium iodide labelled samples were compared to the labelling of the other eight fluorescent dyes, only propidium iodide labelling was stable in chloral hydrate, with the other dyes showing moderate to rapid leaching of dye from the walls giving reduced wall labelling and higher backgrounds (data not shown). We tested whether the acidic nature of the chloral hydrate media (pH ~2.0) caused reversal of the covalent bonding in the pseudo-Schiff reaction by adjusting the pH of the choral hydrate solution to pH 8.0 with concentrated NaOH. While this caused a marked reduction in the leaching of most dyes, it did not eliminate the problem. Instead, we found that 100% glycerol provided a suitable, high refractive index mounting agent in which dye leaching from the cell walls was minimised (Table 1). The high refractive index and pH 10 ClearSee solution (Kurihara et al. 2015) was also compatible with both propidium iodide and rhodamine-123 labelling (data not shown).

*Rhodamine-123 provides a preferred alternative to propidium iodide for cell wall imaging*

Of the alternative Schiff-like dyes tested, several contenders to complement or replace the use of propidium iodide in the labelling of plant cell walls were found after optimisation of labelling conditions. Auramine O and safranin O both performed as well as propidium iodide, but these dyes can also bind directly to the cell wall without undergoing a pseudo-Schiff reaction (Srebotnik and Messner 1994, Ursache et al. 2018). Rhodamine-123, however, provided a superior alternative to propidium iodide for labelling plant cell walls via the pseudo-Schiff reaction when prepared in water at a final concentration of 1.0 µg/mL. Under these conditions, rhodamine-123 gave consistently brighter labelling of cell walls compared to propidium iodide (at 10 µg/mL diluted in water), with brightness values of ~640 for rhodamine-123 compared to ~575 for propidium iodide (Fig. 2B). We tested whether this improved fluorescence labelling generated better images by investigating wall ingrowth deposition in phloem parenchyma transfer cells of cotyledons. This increased fluorescence intensity resulted in lower noise within the rhodamine-123 images and gave consistently sharper imaging of the reticulate wall ingrowths. At lower magnifications, rhodamine-123 labelling of the vascular tissue (Fig. 4B) was similar to propidium iodide (Fig. 4A), but at higher magnifications the improved image resolution provided by rhodamine-123 was apparent, with the wall ingrowths in the phloem parenchyma transfer cells consistently being more clearly defined (Fig. 4F). This improved resolution was also apparent in orthogonal sections generated from Z-stacks collected with the pinhole minimised, an approach that increased resolution in the Z-direction by decreasing the thickness of each optical section (Pawley 2006). Relatively little difference was apparent at low magnification where both propidium iodide (Fig. 4C) and rhodamine-123 (Fig. 4D) enabled imaging through entire leaves, and in some cases, propidium iodide gave better cross sections. However, the vascular bundle in the propidium iodide sample generated a shadow in the upper half of the leaf because the labelled tissue more strongly absorbed the excitation laser (Fig. 4C, asterisk). In higher magnification orthogonal images, the detail of wall ingrowth deposition in phloem parenchyma transfer cells (Fig. 4H, arrows) adjacent to sieve elements (arrowheads) was markedly better with rhodamine-123 compared to propidium iodide.

*Super-resolution imaging of cell walls with STED*

The wall ingrowths of phloem parenchyma transfer cells provide a challenge for conventional confocal imaging because the diameters of these intricate finger-like invaginations and the spacing of these structures in the reticulate array is only slightly larger than the resolution of confocal imaging systems. Thus, wall ingrowths are an ideal system to be imaged by super-resolution microscopy. Our need to investigate the chemistry of the Schiff reaction arose, in part, from our observation that propidium iodide was not compatible for STED imaging on the available imaging system. The super-resolution imaging in this study was performed with a Leica SP8 STED system equipped with 592 nm and 775 nm depletion lasers, but lacked a 650

nm depletion laser available on some other systems. When using the 592 nm STED depletion laser, we observed strong anti-Stokes excitation (STED-light-induced fluorescence) because of propidium iodide's broad excitation spectrum, and high levels of background noise were also observed. When the 775 nm depletion laser was used, propidium iodide was not efficiently depleted even when used at high laser powers, and there was no resolution improvement while considerable background noise also remained. We envisage that propidium iodide would have not been effectively depleted with a 660 nm laser either due to the dye poor de-excitation efficiency in STED microscopy, and found no examples in the literature of this dye having been used successfully in STED imaging.

We also tested whether rhodamine-123 could be imaged by STED microscopy. Using the 592 nm depletion laser, we observed no increase in resolution when using low to medium laser powers. A weak gain in resolution was obtained when using higher STED laser power, but this increase was associated with a more pronounced photobleaching. Moderate higher resolutions were obtained when using the 775 nm depletion laser, which indicates that rhodamine-123 has a larger de-excitation efficiency at that wavelength. However, this superior resolution was limited by the photobleaching of the probe during 3D-STED imaging (data not shown). Wang and colleagues reported that rhodamine-123 was photobleached during STED imaging when using a depletion laser at 660 nm (Wang et al. 2019). Perhaps the STED pulse duration of commercially available STED systems do not allow optimal de-excitation of rhodamine-123 to occur.

ATTO dyes are, however, suitable for STED imaging (Willig et al. 2007, Sednev et al. 2015), and being available as amine derivatives, we investigated these as alternatives. As with the other alternative Schiff dyes tested, the labelling of both ATTO dyes was considerably weaker when dissolved in the pseudo-Schiff solution, and in the case with ATTO 647N-amine, almost no labelling was detected (data not shown). However, when ATTO 565-amine and ATTO 647N-amine were diluted in water to 1.0 µg/mL, they successfully labelled oxidised Arabidopsis cotyledons with fluorescence intensities matching those of rhodamine-123 (1.0 µg/mL) and propidium iodide (10 µg/mL) (Table 1).

STED 660-nm and 750-nm depletion lasers are recommended for ATTO565 and ATTO647N, respectively, but since a 660-nm depletion laser was not available for this study, only samples labelled with ATTO 647N-amine were imaged by STED. Arabidopsis cotyledons labelled with ATTO 647N-amine were imaged by conventional confocal microscopy, with wall ingrowths appearing blurred in both single sections and in maximum projections covering a depth of 5 µm (Fig. 5A, arrowhead). Resolution was clearly improved by STED imaging with individual

ingrowth papillae becoming visible (Fig. 5B). Resolution was further improved by applying deconvolution with the Huygens Professional software package which enhanced the imaging of the tangled network of ingrowth papillae, emphasising the reticulate nature of wall ingrowths in these transfer cells (Fig. 5C, arrows). These deconvolved STED images approached the detail of wall ingrowth deposition produced by scanning electron microscopy (see Figure 3b in Edwards et al. 2010), and thus make it possible to explore the nature of the wall ingrowths in 3D.

A second example of the improvements in resolution for wall ingrowths achievable by STED imaging and deconvolution is shown in Fig. 6. While individual focal planes and a projection of a Z-stack of the STED images show impressive detail of phloem parenchyma wall ingrowths (Fig. 6A, C), deconvolution allows the full complexity of the network to be better understood (Fig. 6B, D). Furthermore, while understanding the organisation of the primary cell wall in parenchyma cells was not an aim of this project, both STED imaging and, notably, deconvolution showed textured cell walls indicating that individual cellulose microfibril bundles might be on the verge of being resolved with this approach (Fig. 6E-H).

*Measuring plasma membrane surface areas associated with cell wall ingrowths*

The improved resolution provided by STED imaging and deconvolution made it possible to produce detailed 3D surface-rendered reconstructions of wall ingrowths using the 3D module in the Leica Application Suite X (LAS X) software, and to quantify the increase in plasma membrane surface area associated with wall ingrowth development. This analysis makes the assumption that the surface area of the cell wall ingrowths matches the surface area of adjacent plasma membrane (Fig. 7). It is this increase in plasma membrane surface area associated with intricate wall ingrowth networks, coupled with the corresponding increased density of membrane transporters that allow transfer cells to increase nutrient transport (McCurdy et al. 2008).

First, the relative size of wall ingrowths was measured. Over various stages of development, tubular ingrowths averaged about 0.35 µm in width. Regions of phloem parenchyma that contained wall ingrowths at varying stages of development and were approximately 2 µm wide and 10 to 20 µm in length were cropped out of larger Z-stacks (Fig. 7A, D, G), and subjected to thresholding so that only the wall ingrowths remained in the image. The relative depths within the images were colour-coded to emphasise the 3D nature of the images (Fig. 7B, E, F). The 3D nature of the wall ingrowths, and the increased complexity of the structures as they develop, is demonstrated in Supplementary movies 1-3 which correspond to Fig. 6B, E and H.

These thresholded images were then surface-rendered, and the surface area of the resulting objects measured.

While the measured surface area varied considerably with the thresholding conditions used, the analysis confirmed increased surface areas associated with wall ingrowth development. In a phloem parenchyma transfer cell in the early stages of ingrowth formation, and which was running at a slight angle across the image frame (Fig. 7A-C), eight ingrowth regions were detected, corresponding to depths of about 1 μm. After thresholding (Fig. 7B), surface rendering (Fig. 7C) demonstrated that surface area more than doubled from 20 to 44 $\mu m^2$. Similarly, in a more complex set of wall ingrowths, the eight detected regions increased surface area from 35 to 150 $\mu m^2$, an increase of approximately 300% (Fig. 7D-F). In the most complex wall ingrowths, which cover a depth of up to 2.0 μm, only four distinct shapes were detected because of the merging of separate ingrowths. In this example, surface area increased from 25 to 164 $\mu m^2$, an increase of more than 500% (Fig. 7G-I). These estimates, however, are likely to underestimate plasma membrane surface areas because even STED microscopy cannot image the finest details of wall ingrowths, and some of the smaller ingrowth details were likely lost during thresholding and rendering.

## Discussion

We have identified several alternatives to propidium iodide that are fluorescent, and act as Schiff-like dyes suitable for pseudo-Schiff labelling of plant cell walls that label when the coupling reaction was performed at a neutral pH rather than the traditionally used, low-pH pseudo-Schiff solution. These improvements allowed for much lower dye concentrations, provided improved images when rhodamine-123 was used, and proved critical for the adaptation of the Schiff reaction for use with the amine-derivative of the ATTO-647N dye for confocal and STED super-resolution microscopy.

### *The chemistry of the Schiff reaction*

Our improved understanding of Schiff reaction chemistry, coupled with the successful identification of alternative Schiff dyes, demonstrated that the low pH pseudo-Schiff solution traditionally used to dilute propidium iodide in cell wall labelling (Haseloff 2003, Truernit et al. 2008, Wuyts et al. 2010) is not only unnecessary, but actually diminishes the reaction. Instead, the coupling reaction should be run at a neutral pH in water. Furthermore, we also found that for dyes other than propidium iodide, the covalent bonds formed during the labelling process were cleavable under acidic conditions. Thus, glycerol was identified as a preferred mounting

medium instead of the highly acidic and toxic chloral hydrate mounting solution. Similar improved results were also achieved by mounting stained tissue in the alkaline ClearSee mounting medium which contains xylitol, urea and sodium deoxycholate (Kurihara et al. 2015). The benefits of removing the acid-based pseudo-Schiff solution from the reaction have been noted previously, making it surprising that this acidic solution has remained in use. Acriflavine, for example, labelled more strongly in a Schiff-reaction when the pseudo-Schiff solution was substituted with 90% ethanol (Levinson et al. 1977). Furthermore, in organic chemistry, Schiff base reactions are typically conducted in either methanol or DMSO, with the addition of a weak acid to create optimal pH 4-6 conditions (Bhagat et al. 2013, Mak et al. 2017).

*Rhodamine-123 as a preferred pseudo-Schiff reagent for imaging of cell walls*

Developing an improved pseudo-Schiff protocol enabled us to identify rhodamine-123 as a preferred alternative to propidium iodide, giving consistently better imaging of cell walls of vascular tissue, and in particular resolving the fine detail of wall ingrowths in phloem parenchyma transfer cells . Thus, the improved confocal imaging achieved with rhodamine-123 provided a substantial benefit in visualising the organisation of wall ingrowths. The reason(s) behind the improved image resolution remains unclear. However, the increase in fluorescence even at low dye concentrations, reductions in shadowing within the sample, and the emission for rhodamine-123 has a more tightly resolved peak that lies in the visible part of the spectrum, as opposed to the broad emission for propidium iodide that extends into the near infra-red, might contribute to the better signal to noise ratio seen with rhodamine-123 labelling. Collectively, this improvement achieved by replacing propidium iodide with rhodamine-123 for pseudo-Schiff labelling can be readily applicable for routine confocal imaging of wall structures in other plant cells.

*Deconvolution, Super-resolution and STED imaging of cell wall ingrowths*

Numerous super-resolution methods have been applied to imaging plant samples (reviewed in Schubert 2017, Komis et al. 2018) including several investigations of plasmodesmata (Fitzgibbon et al. 2013, Tilsner et al. 2013, Knox et al. 2015). Several studies have also specifically investigated cell wall structure. A combination of dSTORM (direct Stochastic Optical Reconstruction Microscopy) and TIRF (Total Internal Reflection Fluorescence) microscopy was used to investigate cellulose microfibril organisation in onion epidermis stained with the cellulose specific dye pontamine fast scarlet 4B, an approach that demonstrated differences in microfibril alignment within the thin primary cell wall (Liesche et al. 2013). In a different approach, STED microscopy was used to image lignified secondary cell walls with rhodamine-PEG (Paës et al. 2018). Neither method, however, was suitable for imaging cell walls of tissues embedded deep within organs, such as the cell wall ingrowths

present in phloem parenchyma transfer cells. STED imaging of these structures using ATTO 647N-amine provides a new methodology for detailed observations of cell wall structures in plant cells (Fig. 5-7). It is also likely that cell wall labelling using ATTO 565-amine would also be suitable for STED imaging, with suitable de-excitation lasers. Furthermore, although rhodamine-123 was generally unsuitable for STED imaging, it provides excellent labelling of cell walls for conventional confocal microscopy, and these images were suitable for deconvolution, providing increases in resolution.

STED imaging and subsequent deconvolution was necessary to appreciate the complexity of wall ingrowths in phloem parenchyma transfer cell walls, as their size, 0.2 to 0.35 μm diameter and depth of 1 μm into the cell (Haritatos et al. 2000, Amiard et al. 2005, Maeda et al. 2006, Edwards et al. 2010, Adams et al. 2014, Maeda et al. 2014), approaches the resolution limit of conventional confocal microscopy. The STED microscopy reported here resolved wall ingrowths consistent with these previous measurements, which suggests that STED microscopy might be a practical approach to investigate changes in wall ingrowth deposition as a result of mutation or chemical agents.

*Measuring the increase in plasma membrane surface area*

In addition to providing clearer images of wall ingrowths, the 3D rendering of deconvolved STED images allowed for estimates of the increase in surface area provided by the formation of wall ingrowths. Although such an analysis assumes that the plasma membrane of the cell tightly follows the cell walls as revealed by STED, such estimates are important. To date, few attempts have been made to estimate the increase in surface area provided by wall ingrowth in transfer cells in general, and in *Arabidopsis* phloem parenchyma transfer cells in particular, as measurements need to be interpolated from two dimensional electron micrographs (Adams et al. 2014). However, our estimates of a sixfold increase in plasma membrane surface area, an increase specifically localised to the region of the phloem parenchyma cell wall immediately adjacent to the sieve element, is consistent with a role in sucrose transport out of phloem parenchyma transfer cells and the role of these cells in apoplastic sucrose loading. Our estimates are probably on the low side in comparison to the highly complex cells walls of some other transfer cells, where increases in plasma membrane surface area of up to 20-fold have been reported (Gunning et al. 1970). However, our estimates are on the high side compared to those of Adams and colleagues, who suggested increases in plasma membrane surface area of up to 150% in Arabidopsis (Adams et al. 2014). However, their values were calculated relative to the entire cell surface area of the cell, rather than for the physiologically-relevant regions adjacent to sieve elements where the ingrowths are actually found.

## Conclusions

By removing the unnecessary low pH pseudo-Schiff solution, the pseudo-Schiff cell wall labelling method has been made more efficient with reductions in labelling time at higher pH and reductions in cost due to the reduced dye concentrations used. Furthermore, the improved method also reduces the fragility of samples, a form of disruption previously caused by the low pH solution. In rhodamine-123, this study has revealed a dye that performs consistently better than propidium iodide, which has been the standard for the high-intensity staining of plant cell walls via the Schiff reaction for the past 15 years. These improvements will aid the utility of super-resolution microscopy coupled with deconvolution for imaging plant cell walls, as evidenced by high-resolution imaging of wall ingrowths in phloem parenchyma transfer cells of Arabidopsis.

## Methods

### *Plant material and growth*

*Arabidopsis thaliana* (Arabidopsis) accession Columbia-0 (Col-0) seedlings were grown either on vertically-positioned nutrient agar plates (half-strength Murashige and Skoog medium containing 1% (*v/v*) sucrose and 1.2% (*w/v*) Bacto agar) or directly in potting mix. Seeds germinated on agar plates were surface sterilised using $Cl_2$ vapour (30 min) by placing seeds in a 1.5 mL tube in a desiccator, and by generating chlorine vapour by adding 3 mL of 37% (*v/v*) HCl to 100 mL of bleach in a beaker. Seeds were stratified for two days at 4°C in darkness before being transferred to a growth cabinet (100–120 µmol.m$^{-2}$.sec$^{-1}$, 22°C day/18°C night, 16 h photoperiod). Potted seedlings were watered every second day.

### *Pseudo-Schiff labelling of plant tissue with propidium iodide*

Cell wall labelling was modified from the pseudo-Schiff propidium iodide technique (Nguyen and McCurdy 2015). Isolated cotyledons or whole seedlings between 10 to 20 days old were fixed over night at 4°C in ethanol:acetic anhydride (3:1) and washed twice in 70% (*v/v*) ethanol. Samples were cleared by gentle shaking (3-5 h) in commercial White King™ bleach diluted to 1:3 in water, and washed (30 min) with gentle shaking in a large volume of water. Samples were oxidised in 1% (*v/v*) periodic acid (5 min), washed again in water (5 min) and incubated (~40 min) in propidium iodide solution (1 mg/mL propidium iodide in water diluted to 100 µg/mL in pseudo-Schiff solution [100 mM $Na_2S_2O_5$ and 0.15 M HCl]). Stained samples were washed in water with gentle shaking (10 min) and mounted in chloral hydrate (4 g chloral hydrate, 1 mL

glycerol, 2 mL water) and left exposed to the air overnight before being covered with a coverslip.

*Modifying pseudo-Schiff labelling with alternative Schiff-like reagents*

The standard pseudo-Schiff labelling technique was used with other Schiff-like dyes (basic fuchsin, neutral red, safranin O, toluidine blue, auramine O, rhodamine-123, acriflavine (Sigma, St Louis, MO USA), and ATTO-565-amine and ATTO-647N-amine (Atto-Tec, Siegen, Germany). All dyes were made to 1 mg/mL stock solutions in water, except for the two ATTO dyes (1 mg/mL in dimethyl sulfoxide). Variations to the standard method included, (i) altering the final dye concentrations and varying the staining times, (ii) replacing the acidic pseudo-Schiff solution by dilution of dyes with water, and, (iii) using different mounting agents including 100% (v/v) glycerol or ClearSee buffer, a clearing and mounting agent composed of 10% (w/v) xylitol, 25% (w/v) urea and 15% (w/v) sodium deoxycholate (Kurihara et al. 2015).

*Confocal imaging*

Stained plant tissues were imaged using an Olympus FluoView FV1000 confocal microscope with either a 60x NA 1.35 oil-immersion or 30x NA 1.05 silicone oil-immersion objective. Fluorescent dyes were excited by 483 nm, 559 nm, and 673 nm lasers, with emission wavelengths optimised for each of the dyes used (Table 1). Images (1600 x 1600 pixels) were collected with Kalman averaging set at 5. For Z-stacks, images were recorded with a step size of 250 nm at 3.6x zoom, and with the pinhole minimised to 59 µm. By minimising the pinhole, the thickness of the observed optical section was minimised, and the image resolution in the Z direction improved (Pawley 2006). For experiments involving the quantification of fluorescence, the offset value was set at zero, and the pinhole size set at 133 µm. Focus was adjusted so that the phloem parenchyma strand nearest the abaxial surface of the leaf (and closest to the lens) was in focus (following Nguyen and McCurdy 2015), and the image brightness for the parenchyma maximised without causing saturation by adjusting gain settings. The Olympus FV1000 has two separate gain controls: the control described as “Gain” was also left at a value of 1x, and the control described as “*HV*” was adjusted. This control is equivalent to the gain on most confocal systems, and we describe adjustments in this as a “Gain adjustment.” Comparisons could then be made between image brightness levels based on the gain value required to just reach saturation in the phloem parenchyma. As these gain values are non-linear and inversely correlated with fluorescent intensity, with gain settings being lower for brighter samples, we defined brightness as 1000 minus the gain such that brighter images have higher scores.

*STED imaging*

STED images of tissue stained with ATTO-647N-amine (1 µg/mL) were acquired with a Leica TCS SP8 microscope (Leica Microsystems GmbH, Mannheim, Germany), using a 100x NA 1.40 oil immersion lens, with 647 nm excitation from a tuneable white light laser running at ~1 - 3% for conventional confocal microscopy and 3 - 5% for STED, and with emission wavelengths set between 660 and 750 nm. Fluorescence depletion used a 775 nm laser running at 30-60% output power. The emitted fluorescence intensities were filtered by a notch filter (775 nm). For STED imaging, images (typically 1024 by 1024 pixels) were collected with a pixel size of 25 nm and with a Z-stack step size of 145 nm, and were acquired using sequential scanning with a line average of 2, a frame accumulation of 3 and a scan speed of 600 Hz. Deconvolution of images was performed with Huygens Professional software (Scientific Volume Imaging, Hilversum, The Netherlands).

*Image processing*

Final image processing was carried out using Adobe Photoshop, ImageJ and Huygens Professional software using standard image adjustment tools.

*Image analysis*

In the 3D module of Leica LAS X, the deconvolved STED Z-stacks were rotated so that phloem parenchyma cells containing wall ingrowths ran across the screen. Analyses were limited to cells in which the wall ingrowths were viewed face onwards, and similar processing settings were used for all the cells analysed. The images were cropped such that only the phloem parenchyma cell to be analysed was in the images in the XY, and the Z-stack was limited to only those frames in which the wall ingrowths appeared. Images were then thresholded which removed other cell walls, including the underlying phloem parenchyma primary wall. This was typically possible because the ingrowths were more brightly labelled than most other cell walls. Images were projected, colour coded by depth, small objects (below 1000 voxels in size) removed, and 3D surface rendering applied which allowed the surface area of the ingrowths to be calculated. This area was then added to the area of the underlying cell wall, adjusted such that the approximate area of contact with that wall (estimated by the area of the wall ingrowths in a two dimensional projection) was removed.

## Author contribution

AR and XW conducted the experiments, NFR conducted STED imaging, and NFR and DC performed the surface rendering calculations. AR, DC and DMcC conceived the project and wrote the manuscript. All authors read and approved the final manuscript.


## Acknowledgements

We thank the Australian Centre for Microscopy and Microanalysis at the University of Sydney for access to the Leica SP8 STED system, Suong Nguyen (University of Newcastle) for assistance with several experiments, and Dr. Michela Simone (University of Newcastle) for her valuable advice on the chemistry of the Schiff reaction. XW was supported by a China Scholarship Council (CSC) scholarship. This study was funded by a grant from the Faculty of Science, University of Newcastle.


## Conflict of interest

The authors declare that they have no competing interests.

**Table 1.** Optimised labelling and imaging conditions for fluorescent pseudo-Schiff dyes.

| Dye | mol wt (g/mol) | pKa | Concentration [*1] (µg/mL) | Stain time (min) | Excitation (nm) | Emission (nm) | Mounting agent [*3] | Suitability for STED imaging [*4] |
|---|---|---|---|---|---|---|---|---|
| Acriflavine | 259.7 | 0.26 | 10 | 5 | 473 | 500-600 | G | -- |
| Propidium iodide | 668.4 | 1.57 | 10 | 40 | 559 | 570-670 | CH, G, CS | no |
| Rhodamine-123 | 380.8 | 6.10 | 1 | 40 | 473 | 530-630 | G, CS | possible but not ideal |
| Safranin O | 350.9 | 6.20 | 10 | 5 | 559 | 570-670 | G | -- |
| Neutral red | 288.8 | 6.80 | 10 | 5 | 559 | 570-670 | G | -- |
| Basic fuchsin | 337.9 | 7.03 | 10 | 5 | 559 | 570-670 | G | -- |
| Auramine O | 303.8 | 10.7 | 100 | 40 | 473 | 500-600 | G | -- |
| ATTO565-amine | 781 | unknown | 1 | 40 | 559 | 570-670 | G | probable |
| ATTO647N-amine | 916 | unknown | 1 | 40 | 635, 647 [*2] | 600-700 | G | very good |

[*1] All dyes dissolved in water at neutral pH.

[*2] 647 nm used on the Leica SP8 STED microscope, while 635 nm used on the Olympus FV1000 confocal microscope.

[*3] CH = chloral hydrate; G = glycerol; CS = ClearSee (tested only with propidium iodide and rhodamine-123)

[*4] STED imaging only checked for propidium iodide, rhodamine-123 and ATTO647N-amine.

**Fig. 1. Structures of the Schiff-like dyes.** All dyes illustrated contain free amine groups which can react with aldehyde groups on cellulose microfibrils oxidised with periodic acid. The structure for a ninth dye, ATTO 647N-amine, remains unpublished.

**Fig. 2. Comparison of fluorescence intensity based on optimised gain values for images of the different Schiff reagents.** Brightness in arbitrary units, defined as 1000 minus the gain setting, was measured for images of vascular tissue in oxidised cotyledons of Arabidopsis labelled with each of the seven fluorescent dyes. Dyes are listed in order of their pKa values, starting with acriflavine, the most acidic pKa, with pKa values shown on the figure. Data are means ± standard errors, with images collected from three or more replicate plants. (A) Labelling in pseudo-Schiff solution with 100 µg/mL dye for 40 min. (B) Labelling in either water (black) or pseudo-Schiff solution (grey) using the optimised conditions listed in Table 1.

**Fig. 3. Confocal imaging of vascular tissue in Arabidopsis cotyledons labelled using the pseudo-Schiff reaction.** Images are single optical sections of 13-day old cotyledons labelled with propidium iodide (A, B) and rhodamine-123 (C, D). Images show labelling in water (left column) and the acidic pseudo-Schiff solution (right column) imaged with the same microscope settings to emphasise the increased brightness of labelling achieved using water. Arrows indicate phloem parenchyma transfer cells containing wall ingrowths; x = xylem; m = mesophyll cells; bs = bundle sheath cells. Scale bar = 50 µm for all images.

**Fig. 4. Wall ingrowths in phloem parenchyma transfer cells of Arabidopsis first leaves labelled using the pseudo-Schiff reaction.** Propidium iodide (left column) and rhodamine-123 (right column) labelling used optimal conditions at 10 µg/mL and 1 µg /mL, respectively, and imaged with the pinhole minimised to provide optimal Z-resolution. (A, B) Single optical sections showing short regions of vascular bundles and surrounding mesophyll and bundle sheath cells. (C, D) Orthogonal reconstructions through the entire leaf; images are maximum projections of seven vertical optical sections that represent a depth of 1 µm. Shadowing caused by the vascular bundle was present in the propidium iodide sample (asterisk). (E, F) High magnification, single optical sections showed that wall ingrowths in phloem parenchyma transfer cells were better resolved with rhodamine-123 (F) than with propidium iodide (E). (G, H) Orthogonal reconstructions through the vascular bundle, with rhodamine-123 (H) provided better resolved images than propidium iodide (G). Arrows indicate cell wall ingrowths; arrowheads indicate sieve elements; x = xylem vessels; m = mesophyll cells; bs = bundle sheath cells; ep = epidermis. Scale bar = 50 µm for A - D, scale bar = 10 µm for E - H.

**Fig. 5. High resolution imaging of cell wall ingrowths in phloem parenchyma transfer cells**. Cell wall ingrowths were imaged in phloem parenchyma transfer cells of 10-day old Arabidopsis cotyledon labelled with ATTO 647N-amine. Images show two different locations taken from the same vascular bundle, and are either a single optical section (top row), or a maximum projection through ~15 sections at 145 nm spacing, corresponding to ~2 µm of sample (lower row). Progressive improvements in resolution were apparent from (A, A') confocal images to (B, B') STED imaging and (C, C') deconvolved STED images. This improvement allowed poorly resolved wall ingrowth (arrowheads) to be seen as a complex, and fenestrated 3D network of ingrowths (arrow). Scale bar = 2 µm for all images.

**Fig. 6. STED imaging and deconvolution improve the available resolution of Arabidopsis cell walls**. STED (left column) and deconvolved STED (right column) images are shown for two locations in the same sample of 14-day old cotyledon labelled with ATTO 647N-amine. Phloem parenchyma cell shown as a single plane (A, B) and as a maximum projection of 20 images covering a depth of 3.0 µm (C, D). Phloem parenchyma and an adjacent parenchymal cell as a single plane (E, F) and as a maximum projection of 15 images covering a depth of 2.2 µm (G, H). The local alignment of cellulose faintly visible within the parenchyma cell wall is indicated with double-headed arrows. Scale bar in G = 5 µm for all images.

**Fig. 7. Surface rendering allowed measurements of the surface area of the plasma membrane surrounding wall ingrowths**. Three stages of wall ingrowth development are shown, including newly forming wall ingrowths (A-C), developing ingrowths (D-F), and mature ingrowths (G-I). Areas of ingrowth in phloem parenchyma cells (boxed in top row, A, D, G) were cropped from deconvolved STED images, and shown as maximum projections. These data were thresholded in the 3D module of Leica LAS X (middle row, B, E, H) which are shown as 3D projections, colour coded by image depth. These images were then surface rendered (bottom row, C, F, I), and the surface area of the ingrowth measured and compared to that of the phloem parenchyma cell. See also Supplementary movies 1 to 3. Scale bar in (A) = 5 μm for A, D, G, bar in (C) = 2 μm for B, C, E, F, H and I. Colour bars show image depth in the thresholded and rendered images in μm.

**Supplementary movies 1 - 3.**

3D reconstructions of cell wall ingrowths in phloem parenchyma transfer cells. The improved resolution achieved by STED imaging and deconvolution allowed for the shapes of wall ingrowths to be resolved. The three image sequences show newly forming wall ingrowths (movie 1), developing ingrowths (movie 2) and the highly complex nature of a mature cell wall ingrowth network (movie 3). The ingrowths are colour coded to indicate the depth at which the ingrowths project into the cell. Z stacks were rotated so that the phloem parenchyma cells ran horizontally across the image, and the stacks were then cropped to only include the width of the phloem parenchyma cell. Image thresholding was used to remove background fluorescence and the surrounding primary cell walls leaving only the ingrowths. Surface rendering was used subsequent to this stage to estimate the surface area of the associated plasma membrane. See also Figure 7. Scale bar is 1 μm, and the colour bar indicates depth in the images in μm.

**References**

Adams, W.W., Cohu, C.M., Amiard, V. and Demmig-Adams, B. (2014) Associations between the acclimation of phloem-cell wall ingrowths in minor veins and maximal photosynthesis rate. *Front. Plant Sci* 5: 24.

Amiard, V., Mueh, K.E., Demmig-Adams, B., Ebbert, V., Turgeon, R. and Adams, W.W. (2005) Anatomical and photosynthetic acclimation to the light environment in species with differeing mechanisms of phloem loading. *Proc. Natl. Acad. Sci. USA* 102: 12968-12973.

Anderson, C.T., Carroll, A., Akhmetova, L. and Somerville, C. (2010) Real-time imaging of cellulose reorientation during cell wall expansion in Arabidopsis roots. *Plant Physiol.* 152: 787-796.

Baum, S. (2008) The PAS reaction for staining cell walls. *Cold Spring Harbor Prot.* 2008: pdb.prot4956.

Bhagat, S., Sharma, N. and Chundawat, T.S. (2013) Synthesis of some salicylaldehyde-based Schiff bases in aqueous media. *J. Chem.* 2013: 4.

Chieco, P. and Derenzini, M. (1999) The Feulgen reaction 75 years on. *Histochem. Cell Biol.* 111: 345-358.

Coiro, M. and Truernit, E. (2017) Xylem characterization using improved pseudo-Schiff propidium iodide staining of whole mount samples and confocal laser-scanning microscopy. *Meth. Mol. Biol.*1544: 127-132.

Dapson, R.W. (2016) Schiff and pseudo-Schiff reagents: the reactions and reagents of Hugo Schiff, including a classification of various kinds of histochemical reagents used to detect aldehydes. *Biotechnol. Histochem.* 91: 522-531.

Davis, A.R., Peterson, R.L. and Shuel, R.W. (1986) Anatomy and vasculature of the floral nectaries of *Brassica napus* (Brassicaceae). *Can. J. Bot.* 64: 2508-2516.

Doblin, M., Pettolino, F. and Bacic, A. (2010) Evans Review: Plant cell walls: The skeleton of the plant world. *Funct. Plant Biol.* 37: 357-381.

Edwards, J., Martin, A.P., Andriunas, F., Offler, C.E., Patrick, J.W. and McCurdy, D.W. (2010) GIGANTEA is a component of a regulatory pathway determining wall ingrowth deposition in phloem parenchyma transfer cells of *Arabidopsis thaliana*. *Plant J.* 63: 651-661.

Feulgen, R. and Rossenbeck, H. (1924) Mikroskopisch-chemischer Nachweis einer Nucleinsäure vom Typus der Thymonucleinsäure und die- darauf beruhende elektive Färbung von Zellkernen in mikroskopischen Präparaten. *Hoppe-Seyler´s Z. Physiol. Chem.* 135: 203-248.

Fitzgibbon, J., Beck, M., Zhou, J., Faulkner, C., Robatzek, S. and Oparka, K. (2013) A developmental framework for complex plasmodesmata formation revealed by large-scale imaging of the *Arabidopsis* leaf epidermis. *Plant Cell* 25: 57-70.

Fukunaga, M. and Yielding, L.K. (1980) Co-mutagenic effects of propidium on petite induction by ethidium in *Saccharomyces cerevisiae*. *Mutation Res.* 69: 43-50.

Gunning, B.E.S., Pate, J.S. and Green, L.W. (1970) Transfer cells in the vascular system of stems: Taxonomy, association with nodes, and structure. *Protoplasma* 71: 147-171.

Haritatos, E., Medville, R. and Turgeon, R. (2000) Minor vein structure and sugar transport in *Arabidopsis thaliana*. *Planta* 211: 105-111.

Haseloff, J. (2003) Old botanical techniques for new microscopes. *BioTechniques* 34: 1174-1178.

Haseloff, J., Dorman, E.L. and Brand, A.H. (1999) Live imaging with green fluorescent protein. *Meth. Mol. Biol.* 122: 241-259.

Jensen, W.A. (1962) *Botanical Histochemistry: Principles and Practice,* San Francisco: WH Freeman.

Kapp, N., Barnes, W.J., Richar, T.L. and Anderson, C.T. (2015) Imaging with the fluorogenic dye Basic Fuchsin reveals subcellular patterning and ecotype variation of lignification in *Brachypodium distachyon*. *J. Exp. Bot.* 66: 4295-4304.

Kasten, F.H. (1958) Additional Schiff-type reagents for use in cytochemistry. *Stain Tech.* 33: 39-45.

Kasten, F.H. (1959) Schiff-type reagents in cytochemistry. I. Theoretical and practical considerations. *Histochemie* 1: 466-509.

Knox, K., Wang, P., Kriechbaumer, V., Tilsner, J., Frigerio, L., Sparkes, I. et al. (2015) Putting the squeeze on plasmodesmata: A role for reticulons in primary plasmodesmata formation. *Plant Physiol.* 168: 1563-1572.

Komis, G., Novák, D., Ovečka, M., Šamajová, O. and Šamaj, J. (2018) Advances in imaging plant cell dynamics. *Plant Physiol.* 176: 80-93.

Kurihara, D., Mizuto, Y., Sato, Y. and Higashiyama, T. (2015) ClearSee: A rapid optical clearing reagent for whole-plant fluorescence imaging. *Development* 142: 4168-4179.

Levinson, J.W., Retzel, S. and McCormick, J.J. (1977) An improved acriflavine-Feulgen method. *J. Histochem. Cytochem.* 25: 355-358.

Liesche, J., Ziomkiewicz, I. and Schulz, A. (2013) Super-resolution imaging with pontamine fast scarlet 4BS enables direct visualization of cellulose orientation and cell connection architecture in onion epidermis cells. *BMC Plant Biol.* 13: 226.

Lion, C., Simon, C., Huss, B., Blervacq, A.S., Tirot, L., Toybou, D. et al. (2017) BLISS: a bioorthogonal dual-labeling strategy to unravel lignification dynamics in plants. *Cell Chem. Biol.* 24: 326-338.

Maeda, H., Song, W., Sage, T. and DellaPenna, D. (2014) Role of callose synthases in transfer cell wall development in tocopherol deficient *Arabidopsis* mutants. *Front. Plant Sci.* 5: 46.

Maeda, H., Song, W., Sage, T.L. and DellaPenna, D. (2006) Tocopherols play a crucial role in low-temperature adaption and phloem loading in *Arabidopsis*. *Plant Cell* 18: 2710-2732.

Mak, J.Y.W., Xu, W., Reid, R.C., Corbett, A.J., Meehan, B.S., Wang, H. et al. (2017) Stabilizing short-lived Schiff base derivatives of 5-aminouracils that activate mucosal-associated invariant T cells. *Nature Comm.* 8: 14599.

McCurdy, D.W., Patrick, J.W. and Offler, C.E. (2008) Wall ingrowth formation in transfer cells: novel examples of localized wall deposition in plant cells. *Curr. Op. Plant Biol.* 11: 653-661.

McManus, J.F.A. (1948) Histological and histochemical uses of periodic acid. *Stain Tech.* 23: 99-108.

Mendocilla Sato, E. and Baroux, C. (2017) Analysis of 3D cellular oganization of fixed plant tissues using a user-guided platform for image segmentation. *Bio-Protocol* 7: e2355.

Moreno, N., Bougourd, S., Haseloff, J., Feijó, J.A. (2006) Imaging plant cells. In *Handbook Of Biological Confocal Microscopy*. Edited by Pawley, J.B. ed. pp 769-787. Springer, New York.

Nguyen, S.T.T., Greaves, T. and McCurdy, D.W. (2017) Heteroblastic development of transfer cells Is controlled by the microRNA miR156/SPL module. *Plant Physiol.* 173: 1676-1691.

Nguyen, S.T.T. and McCurdy, D.W. (2015) High-resolution confocal imaging of wall ingrowth deposition in plant transfer cells: Semi-quantitative analysis of phloem parenchyma transfer cell development in leaf minor veins of Arabidopsis. *BMC Plant Biol.* 15: 109.

Paës, G., Habrant, A. and Terryn, C. (2018) Fluorescent nano-probes to image plant cell walls by super-resolution STE microscopy. *Plants* 7: 11.

Pawley JB (2006) Fundamental limits to confocal microscopy. In *Handbook Of Biological Confocal Microscopy*. Edited by Pawley, J.B. ed. pp 20-42. Springer, New York.

Rounds, C.M., Lubeck, E., Winship, L.J. and Hepler, P.K. (2011) Propidium iodide competes with $Ca^{2+}$ to label pectin in pollen tubes and arabidopsis root hairs. *Plant Physiol.* 157: 175-187.

Rui, Y. and Anderson, C.T. (2016) Functional analysis of cellulose and xyloglucan in the walls of stomatal guard cells of Arabidopsis. *Plant Physiol.* 170: 1398-1419.

Schiff, H. (1866) Eine neue Reihe organischer Diamine. *Justus Liebigs Ann. Chemie* 140: 92-137.

Schubert, V. (2017) Super-resolution microscopy - applications in plant cell research. *Front. Plant Sci.* 8: 531.

Schuetz, M., Smith, R. and Ellis, B. (2013) Xylem tissue specification, patterning, and differentiation mechanisms. *J. Exp. Bot.* 64: 11-31.

Sednev, M.V., Velov, V.N. and Hell, S.W. (2015) Fluorescent dyes with large Stokes shifts for super-resolution optical microscopy of biological objects: a review. *Meth. Appl. Fluoresc.* 3: 042004.

Srebotnik, E. and Messner, K. (1994) A simple method that uses differential staining and light microscopy to assess the selectivity of wood delignification by white rot fungi. *Appl. Environ. Microbiol.* 60: 1383-1386.

Stoddard, A. and Rolland, V. (2019) I see the light! Fluorescent proteins suitable for cell wall/apoplast targeting in *Nicotiana benthamiana* leaves. *Plant Direct* 3: e00112.

Suzuki, T., Fujikara, K., Higashiyama, T. and Takata, K. (1997) DNA staining for fluorescence and laser confocal microscopy. *J. Histochem. Cytochem* 45: 49-53.

Tilsner, J., Linnik, O., Louveaux, M., Roberts, I.M., Chapman, S.N. and Oparka, K.J. (2013) Replication and trafficking of a plant virus are coupled at the entrances of plasmodesmata. *J. Cell Biol.* 201: 981-995.

Truernit, E., Bauby, H., Dubreucq, B., Grandjean, O., Runions, J., Barthélémy, J. et al. (2008) High-resolution whole-mount imaging of three-dimensional tissue organization and gene expression enables the study of phloem development and structure in *Arabidopsis*. *Plant Cell* 20: 1494-1503.

Truernit, E. and Palauqui, J.-C. (2009) Looking deeper: Whole-mount confocal imaging of plant tissue for the accurate study of inner tissue layers. *Plant Signal. Behav.* 4: 151-152.

Ursache, R., Andersen, T.G., Marhavy, P. and Geldner, N. (2018) A protocol for combining fluorescent proteins with histological stains for diverse cell wall components. *Plant J.* 93: 399-412.

Wang, C., Taki, M., Sato, Y., Tamura, Y., Yaginuma, H., Okaya, Y., Yamaguchi, S. (2019) A photostable fluorescent marker for the superresolution live imaging of the dynamic structure of the mitochondrial cristae. *Proc. Natl. Acad. Sci. USA* 116: 15817-15822.

Wei, X., Nguyen, S.T.T., Collings, D.A. and McCurdy, D.W. (2020) Sucrose regulates wall ingrwoth deposition in phloem parenchyma transfer cells in Arabidopsis vua affecting phloem loading activity. *J. Exp. Bot. in press*.

Willig, K.I., Harke, B., Medda, R. and Hell, S.W. (2007) STED microscopy with continuous wave beams. *Nature Meth.* 4: 915-918.

Wuyts, N., Palauqui, J.C., Conejero, G., Verdeil, J.L., Granier, C. and Massonnet, C. (2010) High-contrast three-dimensional imaging of the *Arabidopsis* leaf enables the analysis of cell dimensions in the epidermis and mesophyll. *Plant Meth.* 6: 17.

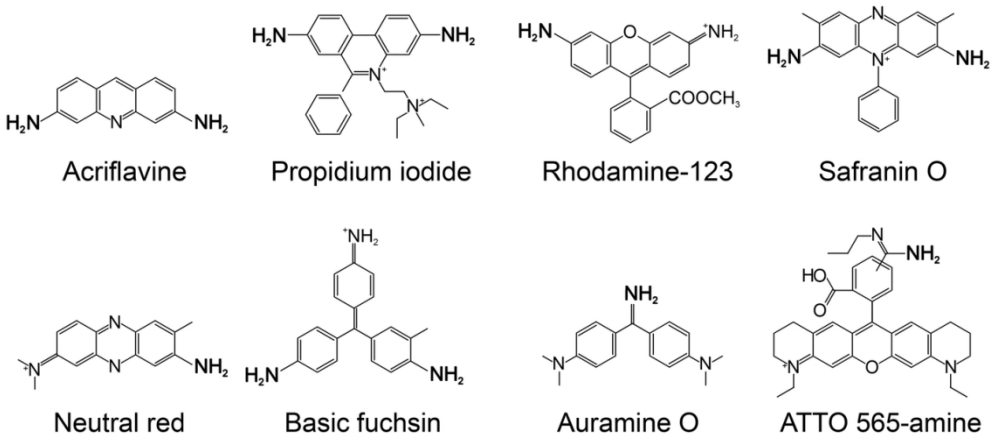


Fig. 1. Structures of the Schiff-like dyes. All dyes illustrated contain free amine groups which can react with aldehyde groups on cellulose microfibrils oxidised with periodic acid. The structure for a ninth dye, ATTO 647N-amine, remains unpublished.

119x56mm (300 x 300 DPI)

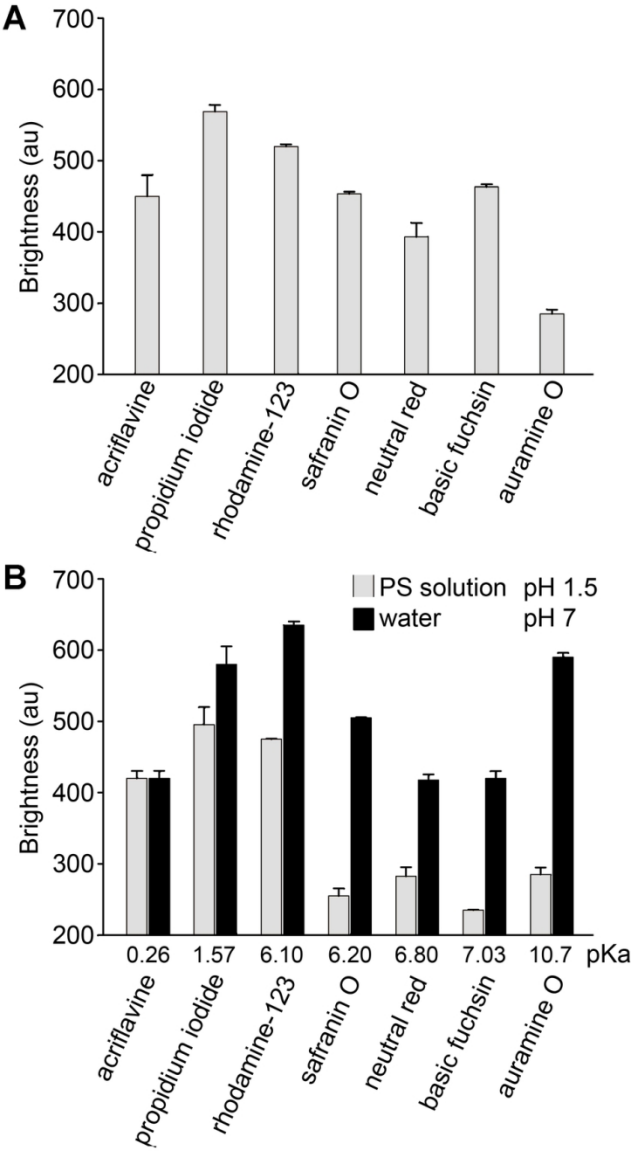


Fig. 2. Comparison of fluorescence intensity based on optimised gain values for images of the different Schiff reagents. Brightness in arbitrary units, defined as 1000 minus the gain setting, was measured for images of vascular tissue in oxidised cotyledons of Arabidopsis labelled with each of the seven fluorescent dyes. Dyes are listed in order of their pKa values, starting with acriflavine, the most acidic pKa, with pKa values shown on the figure. Data are means ± standard errors, with images collected from three or more replicate plants. (A) Labelling in pseudo-Schiff solution with 100 µg/mL dye for 40 min. (B) Labelling in either water (black) or pseudo-Schiff solution (grey) using the optimised conditions listed in Table 1.

80x150mm (300 x 300 DPI)

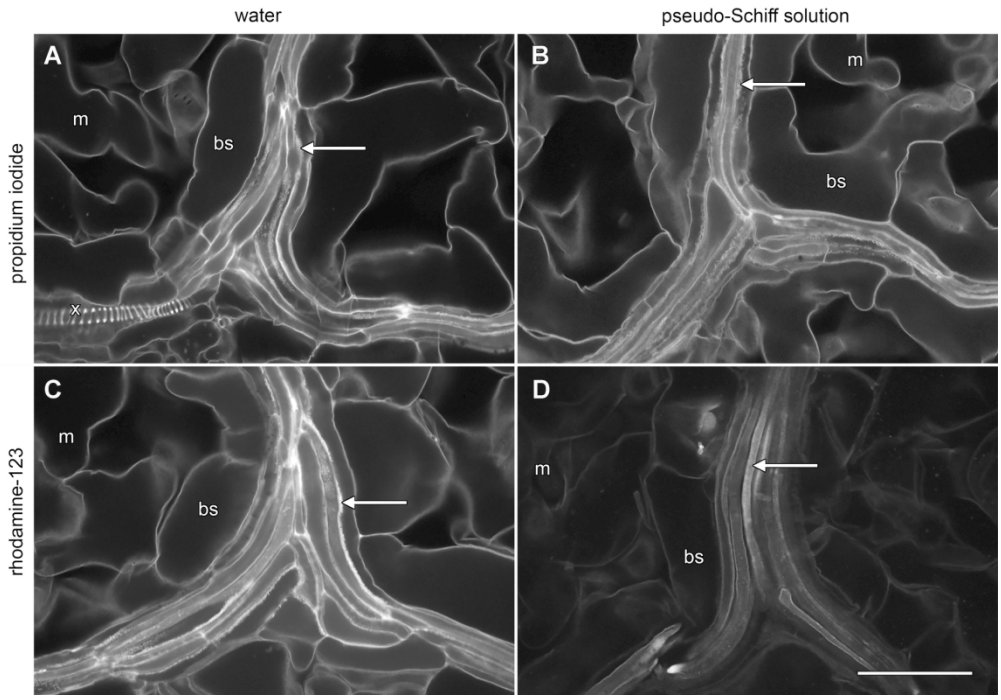


Fig. 3. Confocal imaging of vascular tissue in Arabidopsis cotyledons labelled using the pseudo-Schiff reaction. Images are single optical sections of 13-day old cotyledons labelled with propidium iodide (A, B) and rhodamine-123 (C, D). Images show labelling in water (left column) and the acidic pseudo-Schiff solution (right column) imaged with the same microscope settings to emphasise the increased brightness of labelling achieved using water. Arrows indicate phloem parenchyma transfer cells containing wall ingrowths; x = xylem; m = mesophyll cells; bs = bundle sheath cells. Scale bar = 50 μm for all images.

165x115mm (300 x 300 DPI)

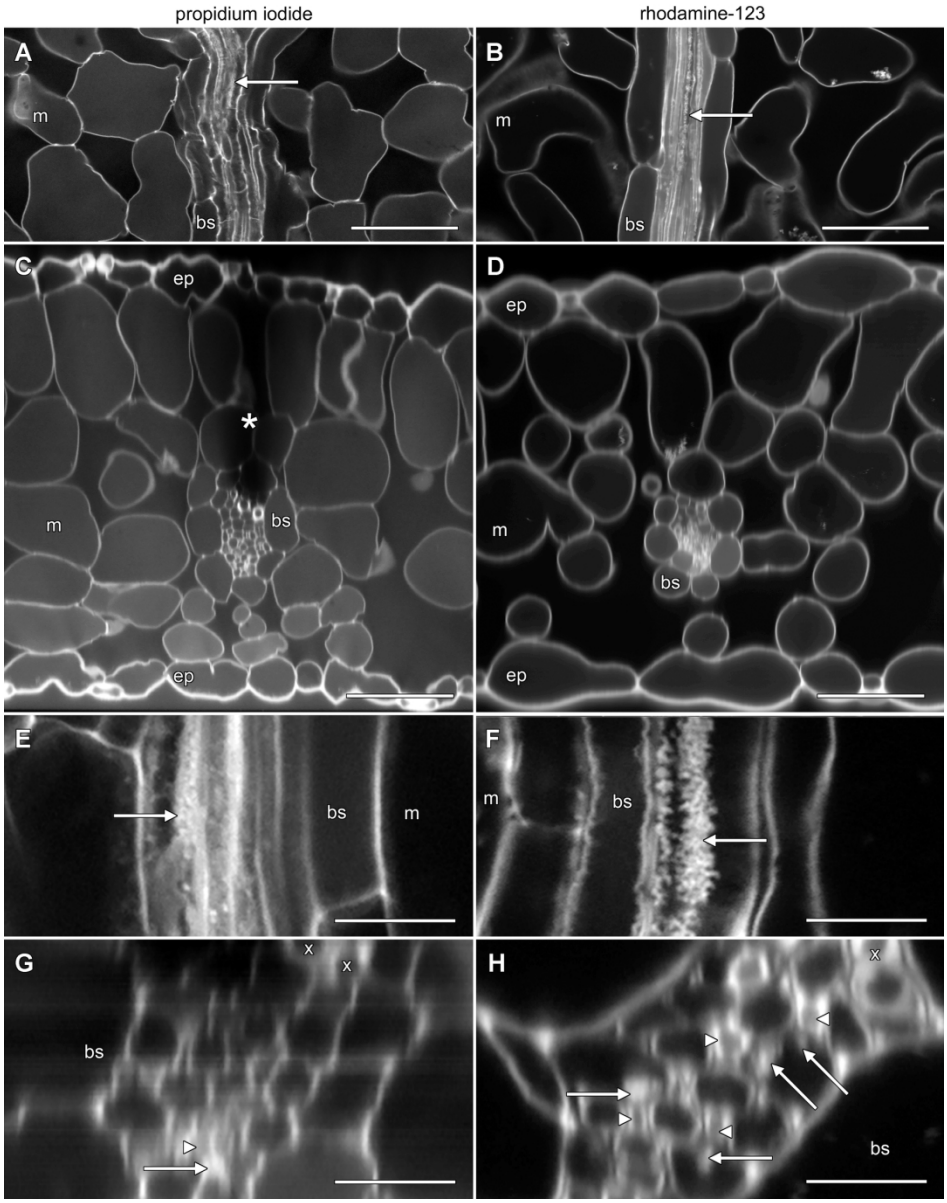


Fig. 4. Wall ingrowths in phloem parenchyma transfer cells of Arabidopsis first leaves labelled using the pseudo-Schiff reaction. Propidium iodide (left column) and rhodamine-123 (right column) labelling used optimal conditions at 10 µg/mL and 1 µg /mL, respectively, and imaged with the pinhole minimised to provide optimal Z-resolution. (A, B) Single optical sections showing short regions of vascular bundles and surrounding mesophyll and bundle sheath cells. (C, D) Orthogonal reconstructions through the entire leaf; images are maximum projections of seven vertical optical sections that represent a depth of 1 µm. Shadowing caused by the vascular bundle was present in the propidium iodide sample (asterisk). (E, F) High magnification, single optical sections showed that wall ingrowths in phloem parenchyma transfer cells were better resolved with rhodamine-123 (F) than with propidium iodide (E). (G, H) Orthogonal reconstructions through the vascular bundle, with rhodamine-123 (H) provided better resolved images than propidium iodide (G). Arrows indicate cell wall ingrowths; arrowheads indicate sieve elements; x = xylem vessels; m = mesophyll cells; bs = bundle sheath cells; ep = epidermis. Scale bar = 50 µm for A - D, scale bar = 10 µm for E - H.

159x203mm (300 x 300 DPI)

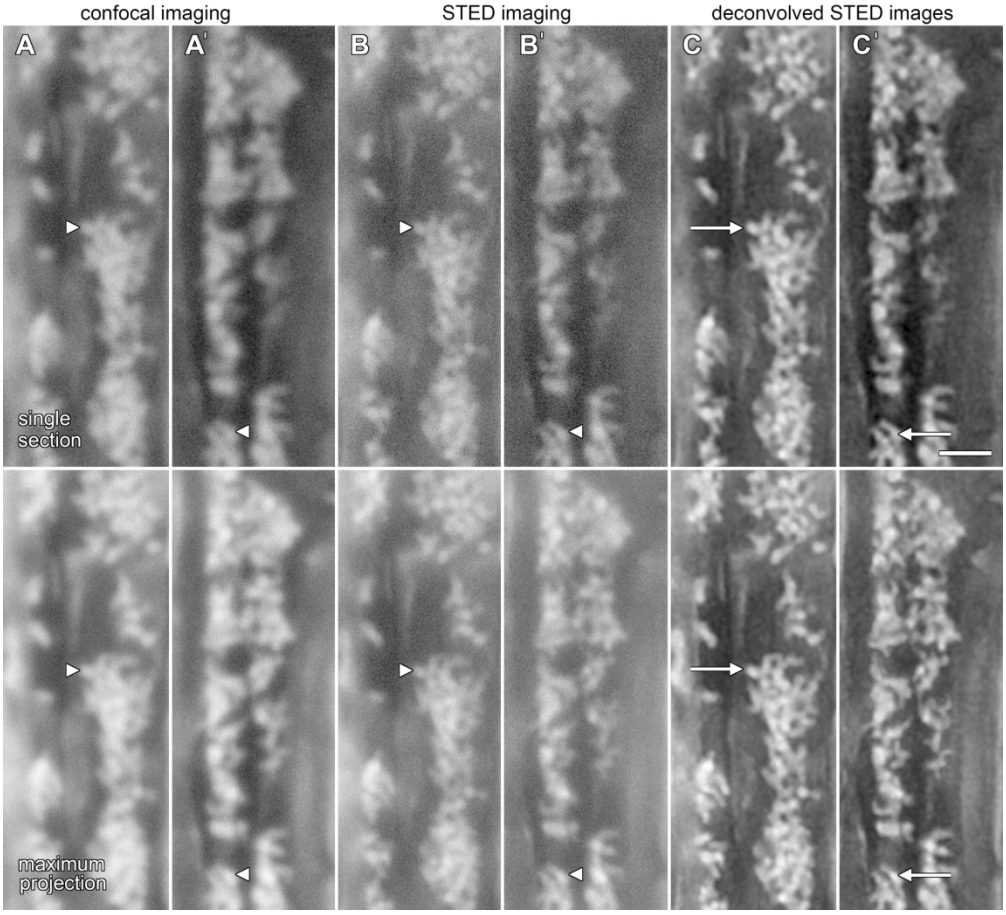


Fig. 5. High resolution imaging of cell wall ingrowths in phloem parenchyma transfer cells. Cell wall ingrowths were imaged in phloem parenchyma transfer cells of 10-day old Arabidopsis cotyledon labelled with ATTO 647N-amine. Images show two different locations taken from the same vascular bundle, and are either a single optical section (top row), or a maximum projection through ~15 sections at 145 nm spacing, corresponding to ~2 µm of sample (lower row). Progressive improvements in resolution were apparent from (A, A') confocal images to (B, B') STED imaging and (C, C') deconvolved STED images. This improvement allowed poorly resolved wall ingrowth (arrowheads) to be seen as a complex, and fenestrated 3D network of ingrowths (arrow). Scale bar = 2 µm for all images.

158x145mm (300 x 300 DPI)

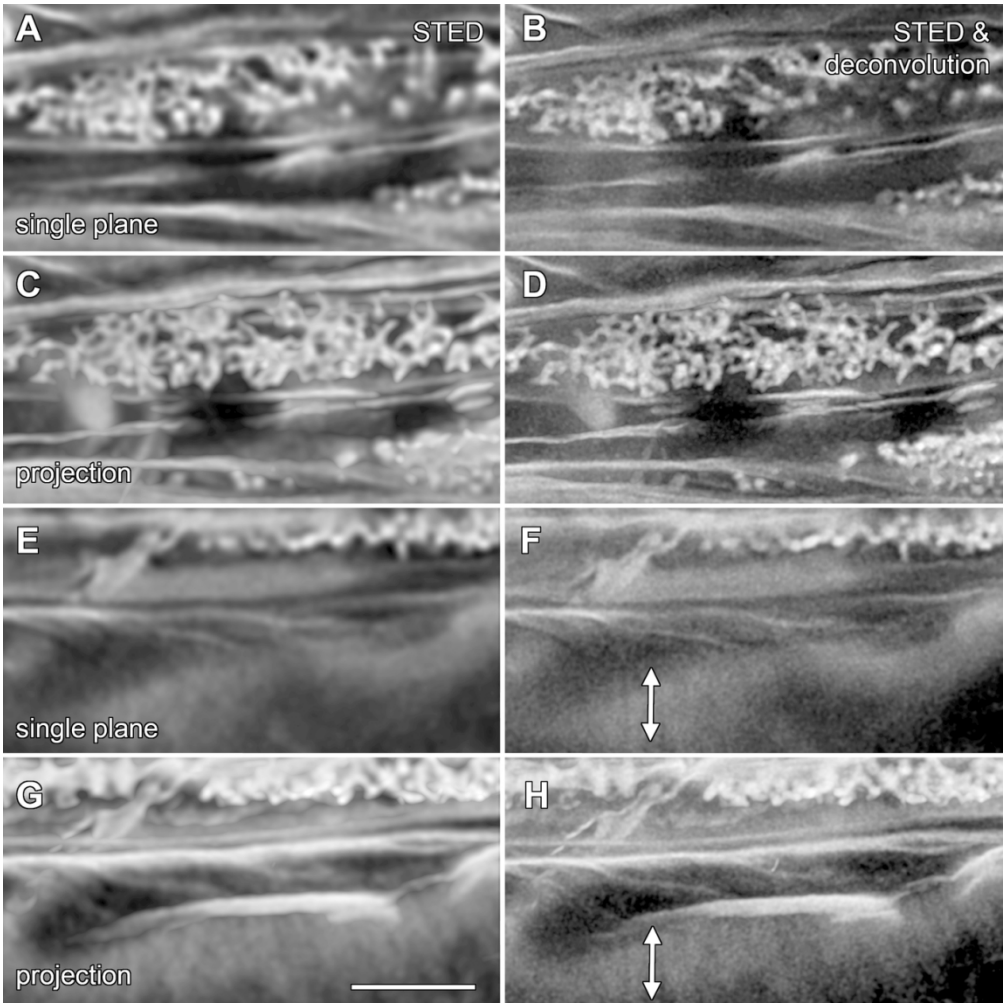


Fig. 6. STED imaging and deconvolution improve the available resolution of Arabidopsis cell walls. STED (left column) and deconvolved STED (right column) images are shown for two locations in the same sample of 14-day old cotyledon labelled with ATTO 647N-amine. Phloem parenchyma cell shown as a single plane (A, B) and as a maximum projection of 20 images covering a depth of 3.0 µm (C, D). Phloem parenchyma and an adjacent parenchymal cell as a single plane (E, F) and as a maximum projection of 15 images covering a depth of 2.2 µm (G, H). The local alignment of cellulose faintly visible within the parenchyma cell wall is indicated with double-headed arrows. Scale bar in G = 5 µm for all images.

118x118mm (300 x 300 DPI)

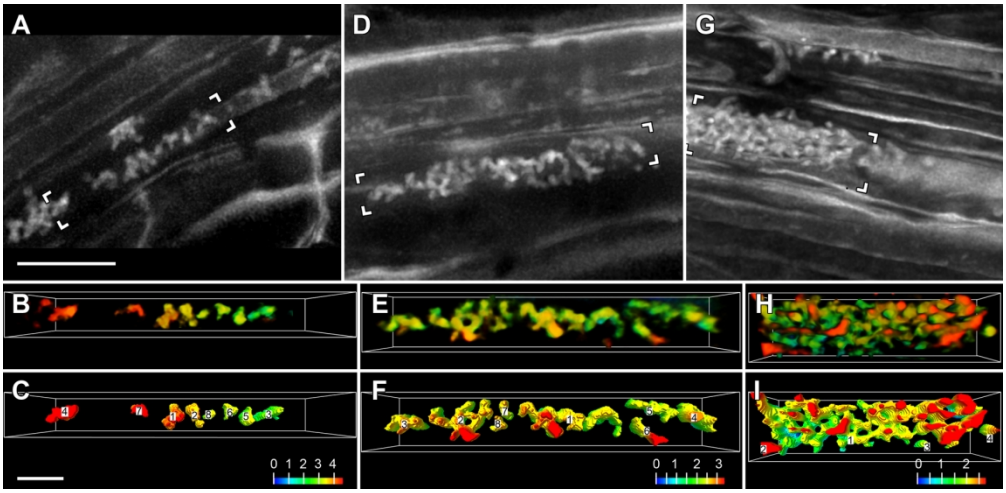


Fig. 7. Surface rendering allowed measurements of the surface area of the plasma membrane surrounding wall ingrowths. Three stages of wall ingrowth development are shown, including newly forming wall ingrowths (A-C), developing ingrowths (D-F), and mature ingrowths (G-I). Areas of ingrowth in phloem parenchyma cells (boxed in top row, A, D, G) were cropped from deconvolved STED images, and shown as maximum projections. These data were thresholded in the 3D module of Leica LAS X (middle row, B, E, H) which are shown as 3D projections, colour coded by image depth. These images were then surface rendered (bottom row, C, F, I), and the surface area of the ingrowth measured and compared to that of the phloem parenchyma cell. See also Supplementary movies 1 to 3. Scale bar in (A) = 5 µm for A, D, G, bar in (C) = 2 µm for B, C, E, F, H and I. Colour bars show image depth in the thresholded and rendered images in µm.

160x77mm (300 x 300 DPI)